Effects of secondary phase and grain size on the corrosion of biodegradable Mg–Zn–Ca alloys

Lu, Yu; Bradshaw, Andrew; Chiu, Y.l.; Jones, I.p.

DOI:
10.1016/j.msec.2014.12.049

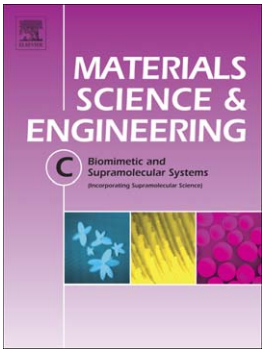

Effects of secondary phase and grain size on the corrosion of biodegradable Mg-Zn-Ca alloys

Y. Lu, A.R. Bradshaw, Y.L. Chiu, I.P. Jones

PII: S0928-4931(14)00847-9
DOI: doi: 10.1016/j.msec.2014.12.049
Reference: MSC 5134

To appear in: *Materials Science & Engineering C*

Received date: 9 April 2014
Revised date: 27 October 2014
Accepted date: 11 December 2014

Please cite this article as: Y. Lu, A.R. Bradshaw, Y.L. Chiu, I.P. Jones, Effects of secondary phase and grain size on the corrosion of biodegradable Mg-Zn-Ca alloys, *Materials Science & Engineering C* (2014), doi: 10.1016/j.msec.2014.12.049

Effects of secondary phase and grain size on the corrosion of biodegradable Mg-Zn-Ca alloys

Y. Lu *, A. R. Bradshaw, Y. L. Chiu, I. P. Jones

School of Metallurgy and Materials, University of Birmingham, Edgbaston, Birmingham, B15 2TT, United Kingdom

ABSTRACT

The bio-corrosion behaviour of Mg-3Zn-0.3Ca (wt%) alloy in simulated body fluid (SBF) at 37 ℃ has been investigated using immersion testing and electrochemical measurements. Heat treatment has been used to alter the grain size and secondary phase volume fraction; the effects of these on the bio-corrosion behaviour of the alloy were then determined. The as-cast sample has the highest bio-corrosion rate due to micro-galvanic corrosion between the eutectic product (Mg + $Ca_2Mg_6Zn_3$) and the surrounding magnesium matrix. The bio-corrosion resistance of the alloy can be improved by heat treatment. The volume fraction of secondary phases and grain size are both key factors controlling the bio-corrosion rate of the alloy. The bio-corrosion rate increases with volume fraction of secondary phase. When this is lower than 0.8 %, the dependence of bio-corrosion rate becomes noticeable: large grains corrode more quickly.

Key words: Mg-Zn-Ca; Degradation; Microstructure; Heat Treatment

1. Introduction

The development of magnesium alloys for biomedical applications is currently under the scientific spotlight. Magnesium alloys have advantages over traditional metallic materials, polymers and ceramics. For example, magnesium alloys have low density (1.74 - 2.0 g/cm^3) and the elastic modulus is about 41 - 45 GPa, which is much lower

than other traditional metallic biomaterials, such as titanium alloys (110 - 117 GPa) and stainless steel (205 - 210 GPa), which is important for avoiding stress shielding. Magnesium alloys are superior to polymers and ceramics in load bearing applications because of their better mechanical properties and fracture toughness. Magnesium is the fourth most abundant cation in the human body and is much involved in the human metabolism and biological mechanisms [1]. In vivo observation of implanted magnesium shows significantly increased bone volume closely formed around the magnesium, indicating good biodegradability [2]. The development of magnesium alloys provides more possibilities for the implants in both un-loaded and loaded applications, such as biodegradable stents [3], screws [4] and intramedullary nails [5]. Although magnesium alloys possess many advantages, their main limitation as biomedical materials is their too high corrosion rate because of their reactive nature (a highly negative standard electrode potential of -2.34 V [6]). Especially, they corrode too quickly in a Cl^- containing solution including human body fluid or blood plasma. Moreover, magnesium alloys are easily attacked by galvanic corrosion. Thus, in order to control the corrosion rate of magnesium alloys, the microstructure - bio-corrosion rate relationship needs to be known.

Zinc is recognized as one of the most abundant and nutritionally essential elements in the human body and therefore is safe for biomedical applications. Zn is beneficial in increasing the tolerance limits of impurities and thus improves the corrosion resistance of magnesium alloys [7, 8]. Also, Zn can improve both the castability (although a high zinc content may cause hot-cracking and microporosity during solidification) and the strength of the alloy. Ca is a major component in human bone and is an important element in cell signalling; released ions are beneficial for bone healing [9]. Ca has a low density (1.55 g/cm^3), which endues the alloy system with a lower density. A high content of Ca is not acceptable because the alloy becomes brittle. Thus, in this work, Zn and Ca have been chosen, set at 3 wt% and 0.3 wt%, respectively. A recent study in the group has shown the effect of very fine precipitates on the bio-corrosion

performance in Mg-3Zn alloy [10]. The volume fraction of nano-scale rod-shaped precipitates increase with ageing time and deteriorates the bio-corrosion resistance of Mg-3Zn. After addition of Ca, the size, morphology and distribution of second phase are changed significantly, which may result in different corrosion rate.

The microstructure generally plays an important role in corrosion behaviour of materials. There have been many studies which focus on the single effect of grain size on the corrosion rate. It has been reported that the corrosion rate decreases with decreasing grain size in some materials, e.g. high purity Al [11], $Ni_{50.5}Ti_{49.5}$ and $Ni_{45.6}Ti_{49.3}Al_{5.1}$ films [12] and pure titanium [13]. Ralston [14] demonstrated that the corrosion rate decreases linearly with decreasing grain size in some metallic alloys. Recent researches indicated that the sole influence of secondary phase on the corrosion rate of magnesium alloys [15-17]. The effects of $Mg_{17}Al_{12}$ (β phase) on the corrosion behaviour of AZ91 alloys have been reported: it can act as either a galvanic cathode and accelerates the corrosion rate, or a corrosion barrier and retards the development of corrosion, which depends on the amount and distribution of the β phase [18, 19]. Magnesium alloys often show different grain size and volume fraction of secondary phases after heat treatments. The corrosion behaviour depends dramatically on these two factors. The works to date have only studied either the relationship between the grain size and the degradation rate or the effects of second phase on degradation rate. However, the combination of secondary phase and grain size in magnesium alloys remains largely unstudied.

In this study, heat treatment was used to modify the grain size and volume fraction of secondary phases without introducing other significant microstructural alteration (such as texture and internal stress). The effect of the volume fraction of secondary phase and of grain size on the resulting bio-corrosion rate of Mg-3Zn-0.3Ca alloy in simulated body fluid (SBF) was then studied.

2. Material and Methods

2.1 Material preparation

Pure magnesium (99.95 wt%), a master alloy (Mg-30 wt% Ca) and pure zinc (99.99 wt%) were used to prepare the alloy. The whole procedure, including melting and casting, was performed in a vacuum induction furnace backfilled with high purity Ar for protection. The chemical composition of the alloy was analyzed with a Rigaku NEX-CG XRF system, to be (in wt%): Zn - 2.97, Ca - 0.33, Si - < 0.0001, Fe - 0.004, Cu - < 0.0001, Ni - < 0.0001, Mg - Balance. The as-cast alloy was solution treated at temperatures ranging from 310 ℃ to 450 ℃ for 24 h and 48 h, followed by water quenching.

2.2 Microstructure

The metallography specimens were polished down to 0.25 μm and then etched in a solution containing 50 ml distilled water, 150 ml ethanol and 1 ml acetic acid. Microstructural observation was carried out using an optical microscope (Zeiss Axioskop) and a scanning electron microscope (Philips XL30 and JEOL JSM-7000F). The grain size was measured using the image analyzer (Axio Vision 4.6.3) based on the Zeiss microscope. Image J was used to analyse the phase volume fraction.

2.3 Immersion test

The immersion test was carried out in Kokubo's simulated body fluid (SBF) [20] at 37 ℃ for up to 10 days. The SBF solution was renewed every 24 h in order to maintain a relatively stable immersion environment. The ratio of SBF volume to sample surface area was 100 mL/cm^2. Samples with dimensions 10 mm ×10 mm ×2 mm were polished down to a surface finish of 1 μm. Three measurements were taken under each condition. The degradation rate was calculated from the volume of hydrogen generated (hydrogen evolution method [21, 22]). The set-up for measuring the hydrogen evolved is shown in Figure 1. Hydrogen bubbles generated from the soaked sample were collected into a measuring cylinder. The amount of hydrogen can be measured from the height difference of the SBF solution in the measuring cylinder. The evolution of one

mole of hydrogen gas corresponds to the dissolution of one mole of magnesium metal, according to the reaction ($Mg + 2H_2O \rightarrow Mg(OH)_2 + H_2 \uparrow$). Thus, the degradation rate of magnesium can by monitored over time via the emitted hydrogen.

After the immersion testing, the soaked specimens were taken out, gently rinsed in deionized water and dried with cool air. The corrosion products were then chemically removed by dipping in 180 g/L CrO_3 solution for 3 mins.

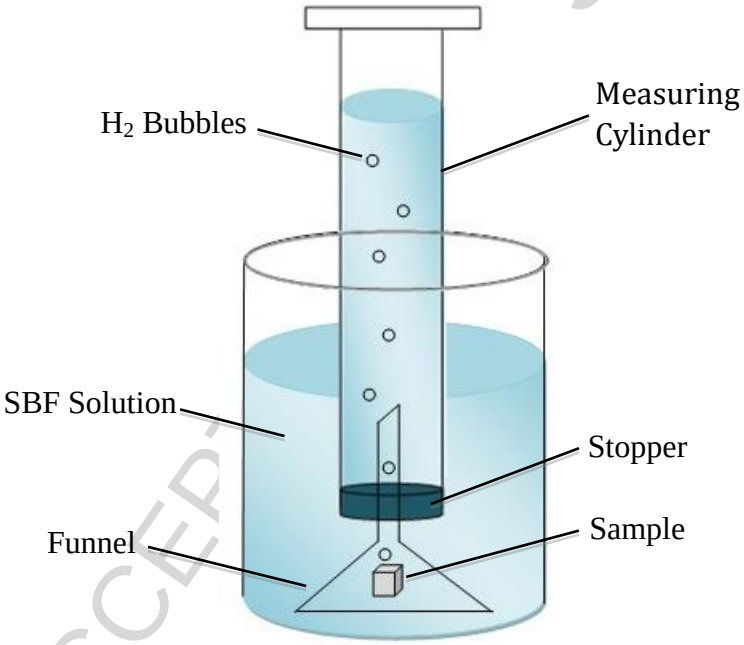

Figure 1 Schematic illustration of measurement of evolved hydrogen volume.

2.4 Electrochemical test

The samples were mounted in epoxy resin with an exposed area of 1 cm^2 and then polished down to 1 μm. The electrochemical test was carried out at 37 ℃ in a beaker containing 100 mL of SBF solution and a standard three-electrode configuration (platinum mesh as counter, saturated calomel as reference and the alloy as working electrode). The working electrode was firstly immersed in SBF for 60 min to measure its Open Circuit Potential (OCP) and then the polarization curve was acquired at a scanning rate of 1 mV/s. The polarization curve was started at a fixed value (50 mV above the OCP) and stopped about -500 mV relative to OCP. Three tests were

performed for each sample condition to investigate the reproducibility of the results.

3. Results and discussion

3.1 Microstructure

As can be seen in Figure 2(a), the as-cast alloy has spherical inclusions and networks along the grain boundaries. A close-up view (Figure 2(b)) shows the eutectic morphology of the particles. The average grain size is 97 ± 6 μm, and the volume fraction of the secondary phase is around 2.4 ± 0.4 %.

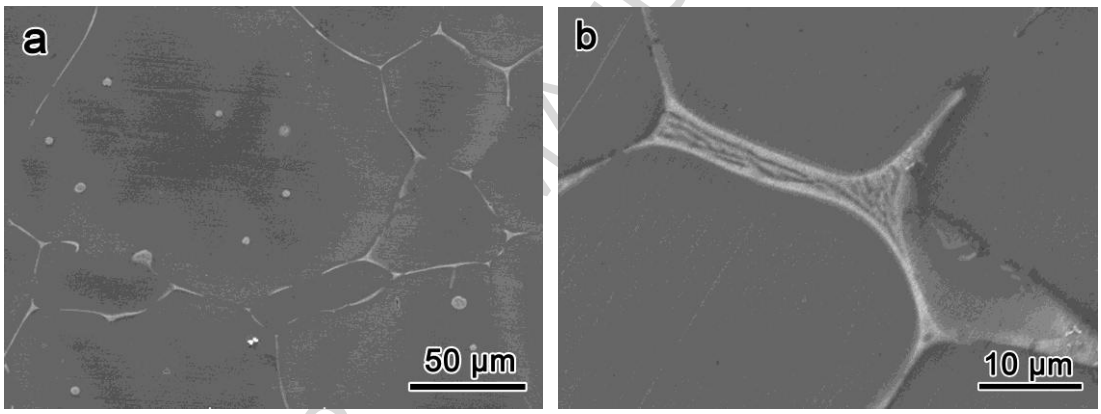

Figure 2 (a) SEM micrograph of the as-cast alloy; (b) SEM micrograph showing the eutectic product along the grain boundaries.

In Figure 3 (a), the globular particle has alternating bright and dark regions. The composition of these precipitates was found to be 60.2 ± 3.7 at% Mg, 15.8 ± 1.5 at% Ca, 24.0 ± 2.3 at% Zn, very close to $Ca_2Mg_6Zn_3$ [23]. The crystal structure of the phase was confirmed by electron diffraction (Figure 3 (b)). The electron diffraction patterns recorded from the dark part of globular particle are consistent with a trigonal unit cell (a=0.97 nm, c=1.0 nm, α=90°, β=90°, γ=120°), reported for the $Ca_2Mg_6Zn_3$ structure [23]. This globular particle is therefore the eutectic (Mg + $Ca_2Mg_6Zn_3$) product.

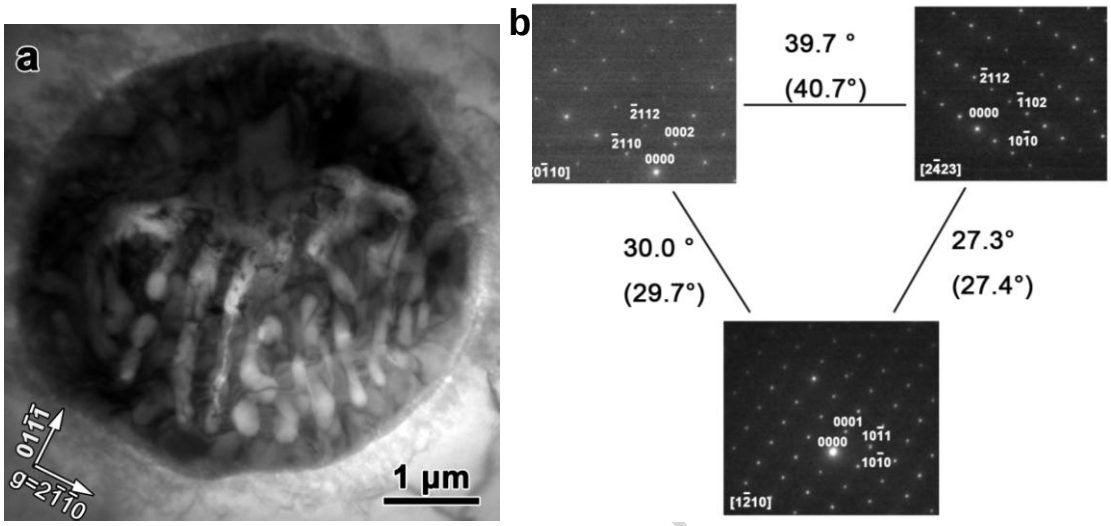

Figure 3 (a) TEM BF image showing a spherical precipitate in the as-cast alloy, BD~ $[01\bar{1}2]$; (b) Electron diffraction patterns confirming the structure of the $Ca_2Mg_6Zn_3$ phase to be trigonal structure. The values without brackets are theoretical tilt angles and the actual tilt angles are shown in brackets.

The strip-like features along the grain boundaries are analysed in Figure 4. They are also confirmed to be (Mg + $Ca_2Mg_6Zn_3$) eutectic product.

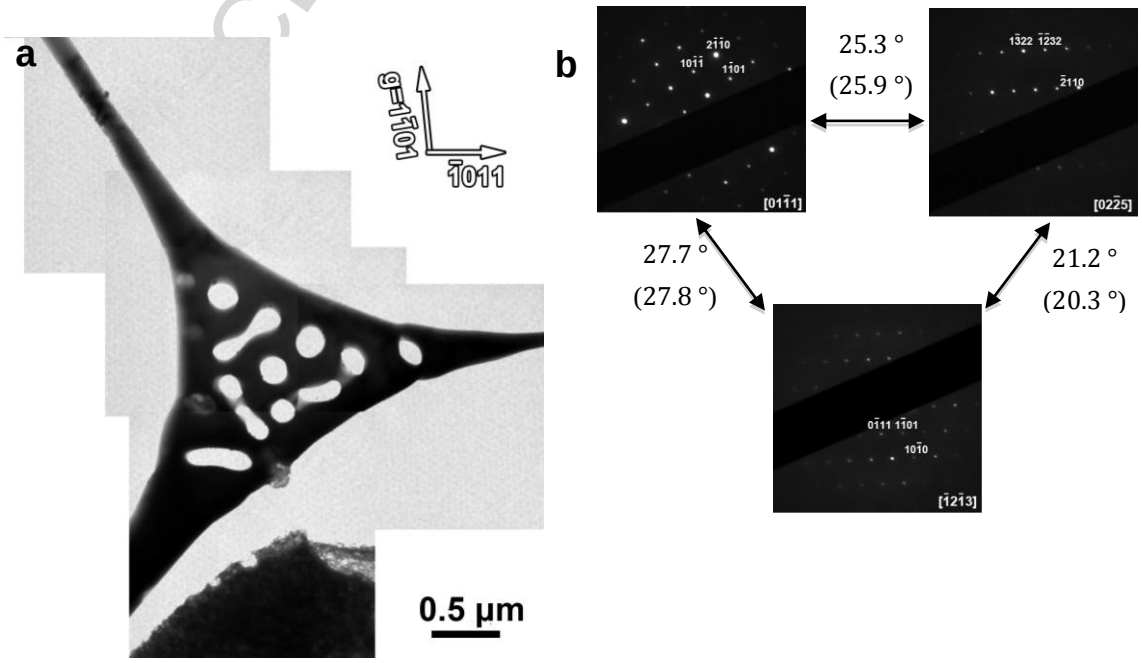

Figure 4 (a) TEM BF image showing a net work located at a grain boundary triple point, the beam direction is close to $[01\bar{1}1]$ of magnesium matrix; (b) Electron diffraction

patterns acquired from the dark region in (a) confirms that its structure agrees with that of the $Ca_2Mg_6Zn_3$ phase. The actual tilt angles recorded in the experiment are shown in the brackets while the theoretical values are shown without brackets.

Figure 5 shows the microstructure of the alloy after different heat treatments. In the as-cast sample, as shown in Figure 5 (a), the dendrite structure is evident. After the treatment at 310℃ for 24 h, the grain size increases (Figure 5 (b)). After the treatment at 360℃ for 24 h, the dendrites disappeared (Figure 5 (c)). The grain size of the sample treated at 400℃ for 24 h has increased further (Figure 5 (d)). In Figure 5(e-h), the grain size increases rapidly with the treatment temperature and time and the amount of the grain boundary secondary phase and the spherical particles reduced. Table 1 summarises the microstructure characteristics of MZX30 after the various solution treatments.

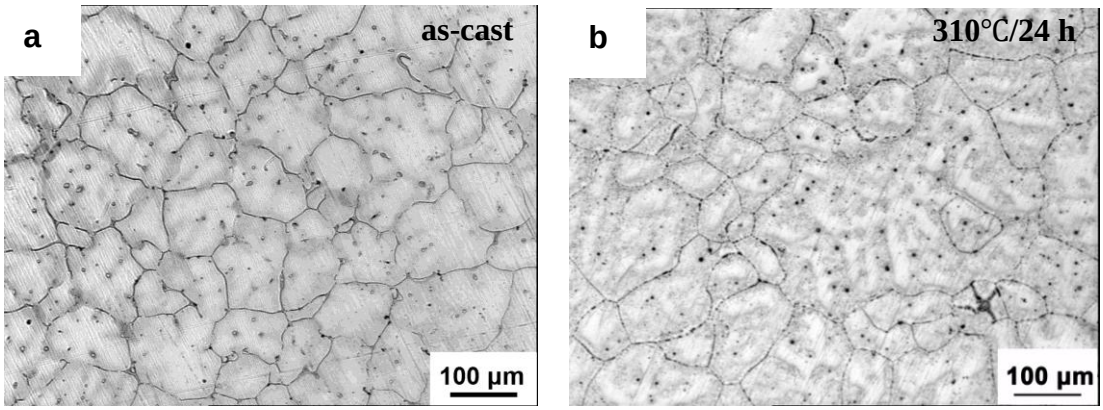

360℃/24 h **400℃/24 h**

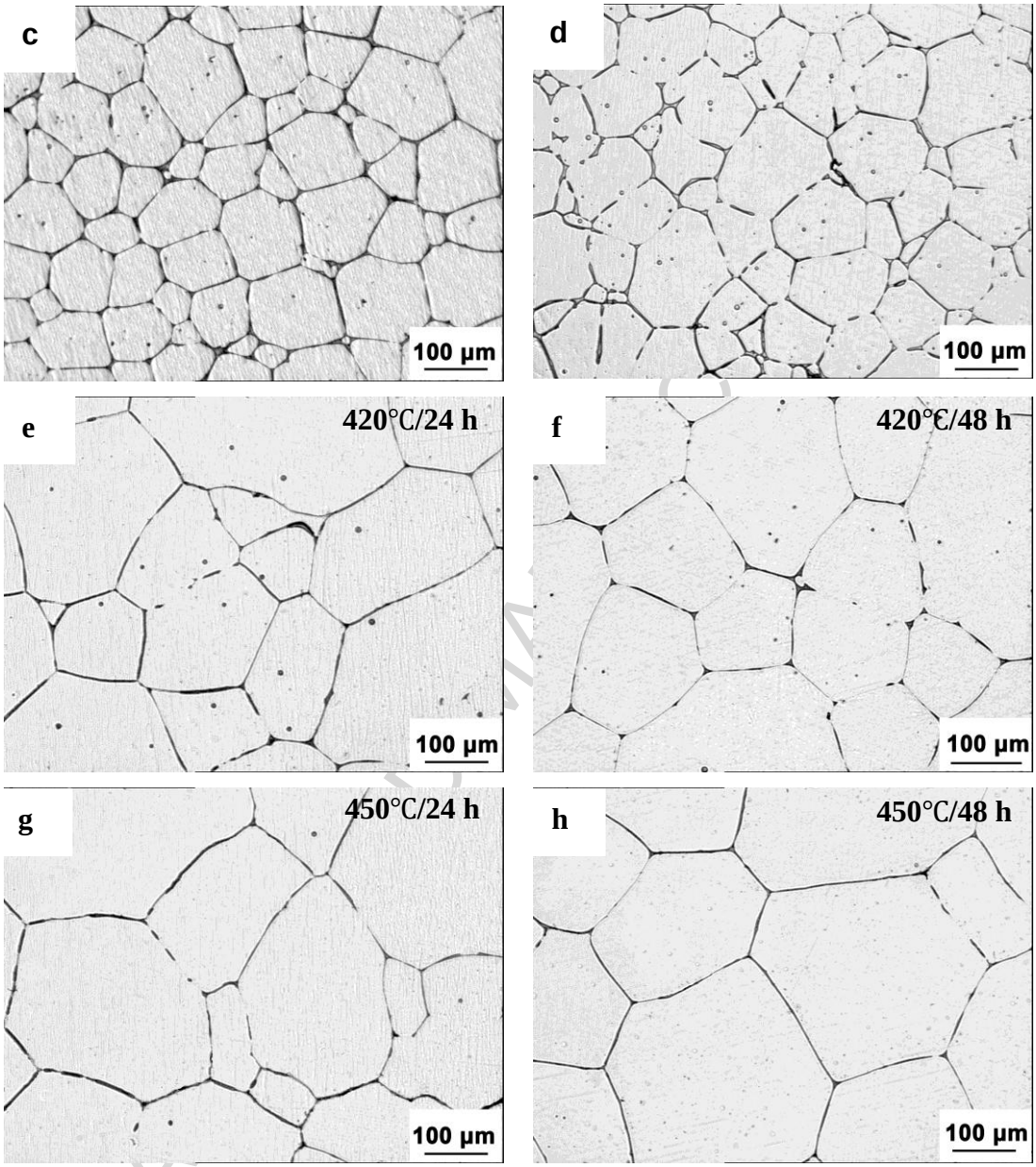

Figure 5 Optical micrographs obtained from the as-cast sample (a) and the heat-treated samples (b-h), showing the microstructure changes (grain size and amount of second phases) upon heat treatment.

Table 1 Microstructure characteristics of the alloys after heat-treatment.

Condition	**Mg-3Zn-0.3Ca**	
	Secondary Phase Volume Fraction (%)	**Grain Size (μm)**
as-cast	2.4 ± 0.4	97 ± 6

310 ℃/24 h	1.7 ± 0.2	114 ± 7
360 ℃/24 h	1.5 ± 0.1	129 ± 9
400 ℃/24 h	1.3 ± 0.3	151 ± 5
420 ℃/24 h	0.7 ± 0.3	166 ± 8
420 ℃/48 h	0.2 ± 0.1	180 ± 7
450 ℃/24 h	0.08 ± 0.03	193 ± 9
450 ℃/48 h	0.06 ± 0.01	214 ± 10

3.2 Influence of heat treatment on degradation rate

The degradation rates of the alloy after heat treatment are shown in Figure 6. In order to display the data clearly, the tolerances are not given in the figure (the maximum tolerance is ± 0.12). After heat treatment, the corrosion resistance of the alloy has improved. It is found that the degradation rate of heat-treated alloy decreases in the order 310 ℃/24 h sample > 360 ℃/24 h > 450 ℃/48 h > 400 ℃/24 h > 450 ℃/24 h > 420 ℃/48 h > 420 ℃/24h. The best corrosion resistance is achieved in the 420℃/24 h treated sample, viz. 1.61 ± 0.09 mL/cm^2/day.

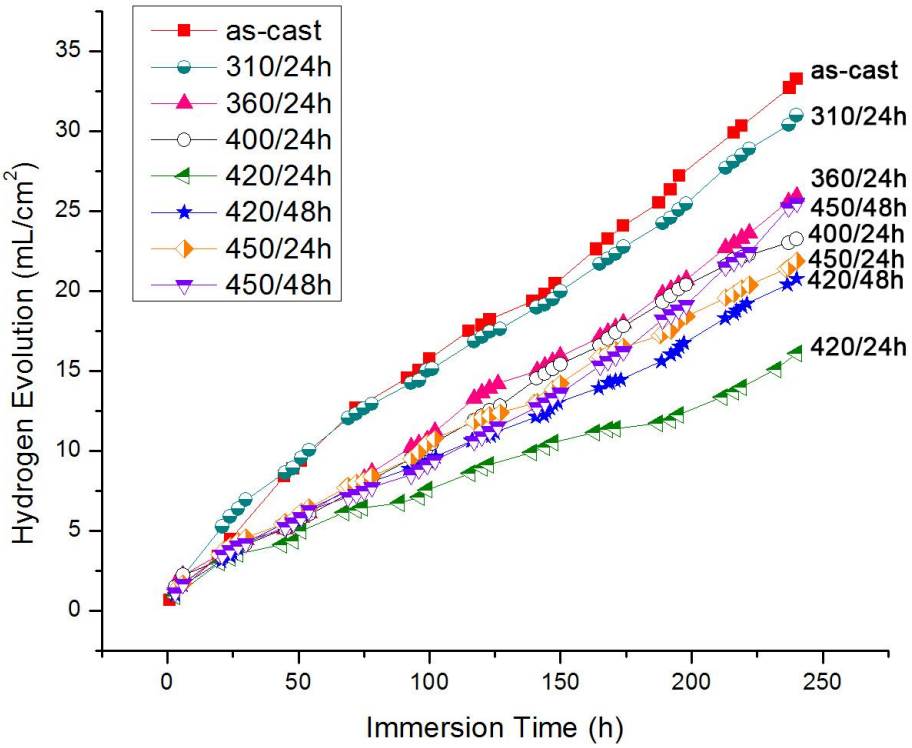

Figure 6 Volume of hydrogen evolved for as-cast and heat treated samples during the 240 h immersion test in SBF.

Figure 7 shows the corrosion morphologies of the alloy after the immersion test. As can be seen in Figure 7(a), the as-cast sample suffered obvious local corrosion attack (pitting), as indicated by the arrows. After heat treatment, the sample shows a smoother corroded surface with fewer pits, as can be seen in Figures 7(b-d). The 310 ℃/24 h treated sample displays less eutectic product and therefore the micro-galvanic corrosion weakens (Figure 7(b)). The sample after 420 ℃/24 h treated sample exhibits a lower density and depth of corrosion pits (Figure 7(e)) and shows the best corrosion resistance. In the 420 ℃/48 h, 450 ℃/24 h and 450 ℃/48 h treated samples (Figures 7(f-h)), a number of tiny corrosion pits on the alloy surface are visible and more corrosion attack occurs in the matrix.

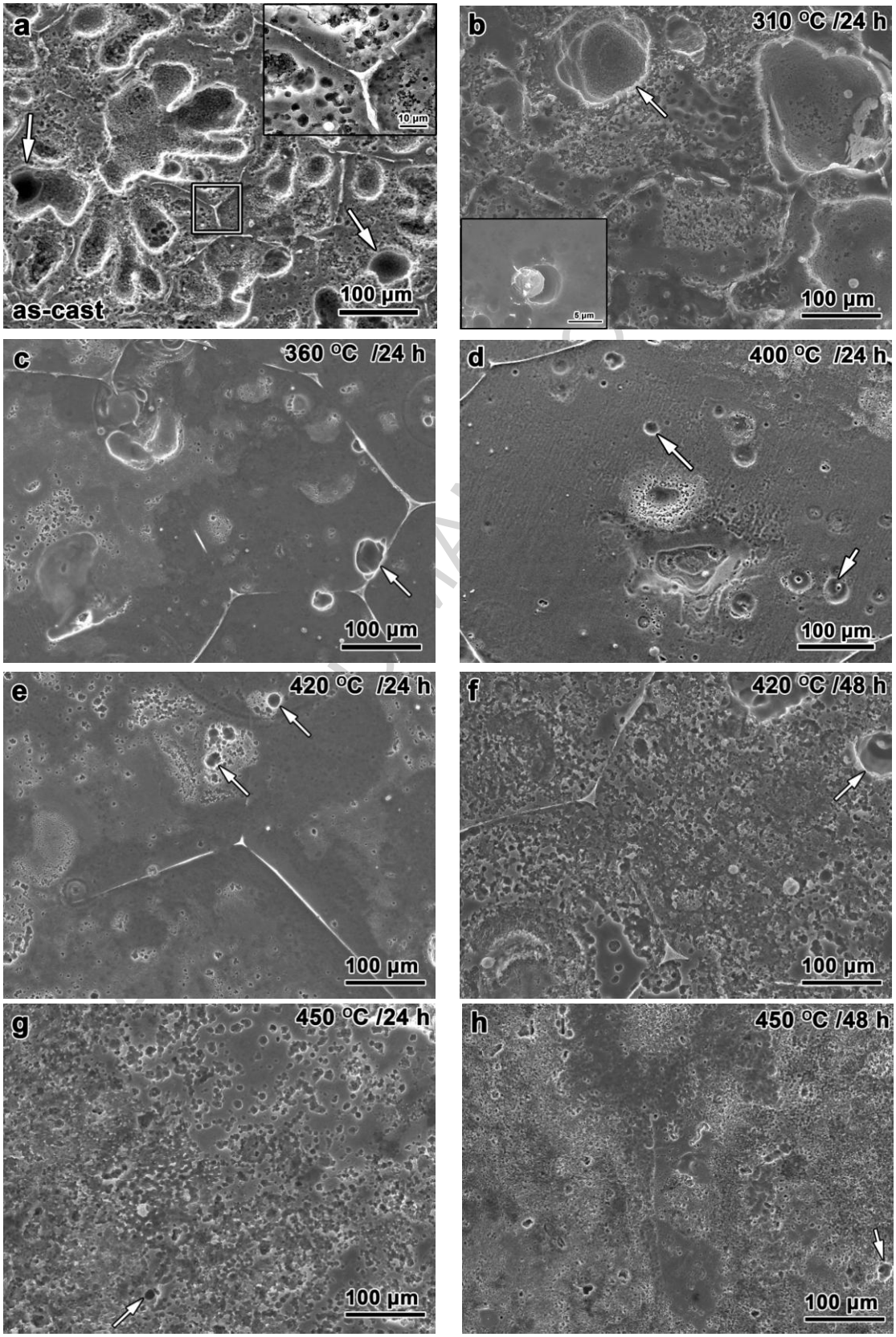

Figure 7 SEM micrographs showing the corroded samples after 10 days' immersion and corrosion product removal. The heat treatment conditions appear in the top right corner in each micrograph.

3.3 Electrochemical testing

Figure 8 shows the evolution of the open circuit potential (E_{ocp}) measured from the alloy samples exposed to SBF solution for 3600 s. Each measurement series started immediately after immersion of the sample in the SBF and reflects the initiation and propagation of corrosion. The curves display a similar tendency over the potential range: a sharp rise initially and then a very slow increase indicating the stable growth of a protective surface film. There was a significant positive shift of E_{ocp} in the heat-treated samples. The 420 ℃/24 h treated sample has a more positive E_{ocp} than the other samples.

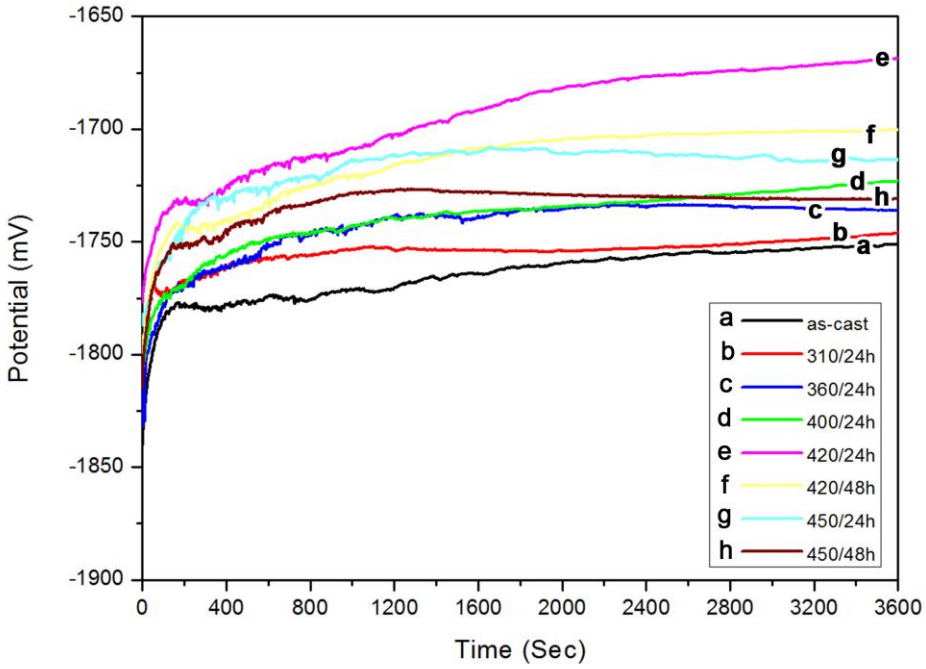

Figure 8 Open circuit potential measurement of alloy samples in SBF at 37 ℃

Figure 9 presents the polarization curves of the samples in SBF at 37 ℃. The as-cast sample shows a more negative value of E_{corr} (-1751.4 mV) and a higher cathodic current density. Noticeably, the cathodic currents from the polarization curves are lower for all heat-treated samples as compared with the as-cast sample. The highest E_{corr} is achieved at 420 ℃/24 h treated sample (-1668.6 mV). The 420 ℃/24 h sample has the lowest cathodic current density, which suggests that the cathodic

reaction resistance has been improved by the heat treatment. Generally, the cathodic polarization curve is assumed to represent the hydrogen evolution from magnesium such that a lower polarization current indicates a lower hydrogen evolution rate. The (Mg + $Ca_2Mg_6Zn_3$) eutectic product acts as a cathode during the micro-galvanic corrosion. More secondary phases thus cause more severe corrosion. This is consistent with the fact that the as-cast sample with the largest volume fraction of secondary phase shows the highest hydrogen evolution rate. The heat treatment leads to a reduction of the amount of secondary phase and thus reduces the corrosion rate.

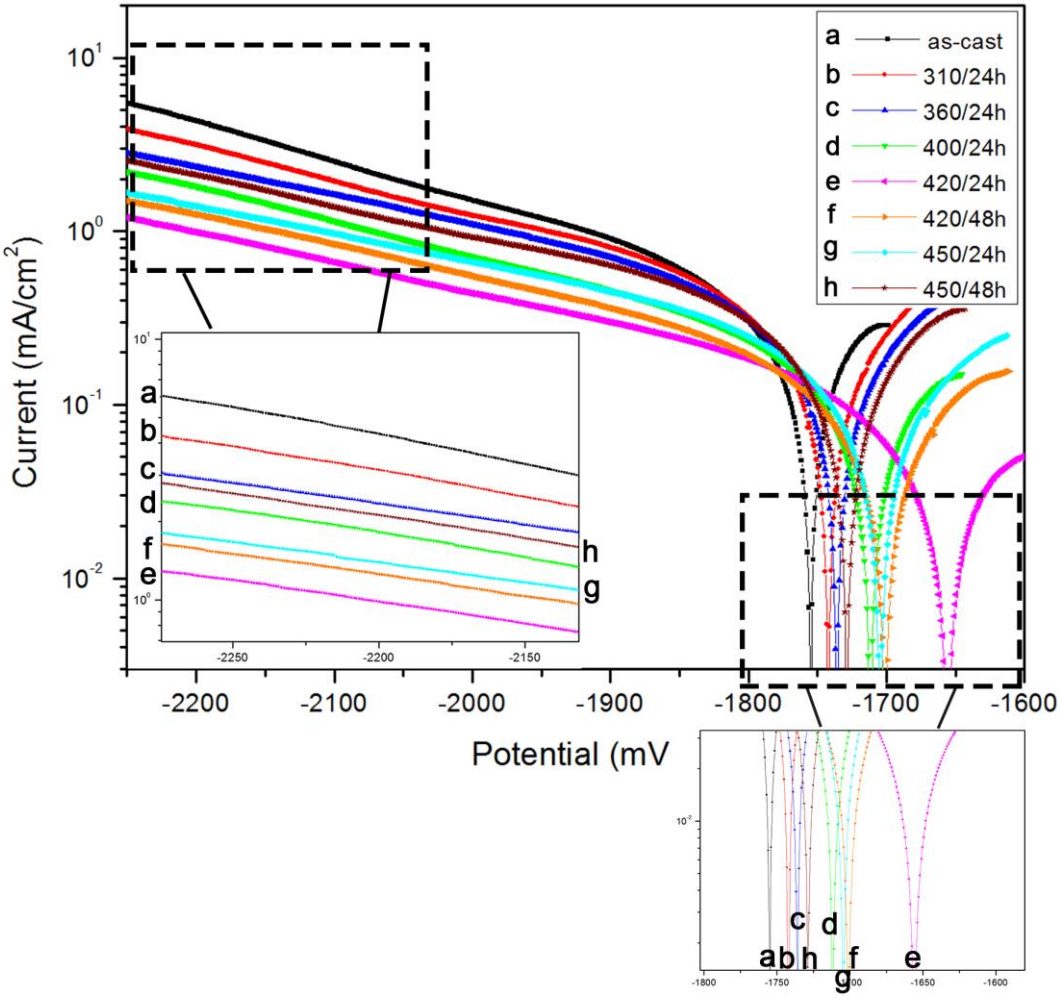

Figure 9 Polarization curves of the samples in SBF at 37 ℃. The inset is an enlarged view of the area highlighted by the dashed square illustrating the different current densities of the samples after heat treatment.

3.4 Effects of microstructure on degradation

The volume fraction of the secondary phase and the grain size in the alloy change with heat treatment, as summarised in Table 1. Figure 10 illustrates the variation of the degradation rate with secondary phase volume fraction and grain size. Each data point presents a measurement of the volume fraction of secondary phase, grain size and the corresponding degradation rate. Figure 10(a) is a plot which combines the effect of both the grain size and the secondary phase volume fraction.

The bio-corrosion rate of this alloy is a function of its grain size and the volume fraction of secondary phase. The amount of secondary phase has been reported to have an obvious impact on the corrosion rate. For instance, i_{corr} increases with an increased density of intermetallic particles [24]. Obviously, the grain boundary secondary phase observed in the current alloys also causes severe galvanic corrosion attack. A homogeneous microstructure without secondary phase is beneficial to corrosion resistance [24]. Grain size affects the corrosion performance of materials. The bio-corrosion rate increases with increasing grain size in the alloy at the higher treatment temperatures (after 420 ℃/24 h). It has also been reported [11, 25, 26] that small grain size is beneficial to the corrosion resistance. The corrosion behaviour is more homogeneous in a fine-grained microstructure because segregation is minimized.

As shown schematically in Figure 10(b), when the grain size and the secondary phase volume faction are both taken into consideration, the combined effect could be like that indicated by the solid curve. Although the as-cast sample has the smallest grain size in the current study, the secondary phase volume fraction is the largest which has clearly overshadowed the beneficial effect of fine grain size on the corrosion performance. While the high temperature heat treated sample has the lowest secondary phase volume fraction, the large grain size of the alloy dominates, such that the corrosion rate is high. The best corrosion performance can be obtained with a balanced grain size and secondary phase volume fraction.

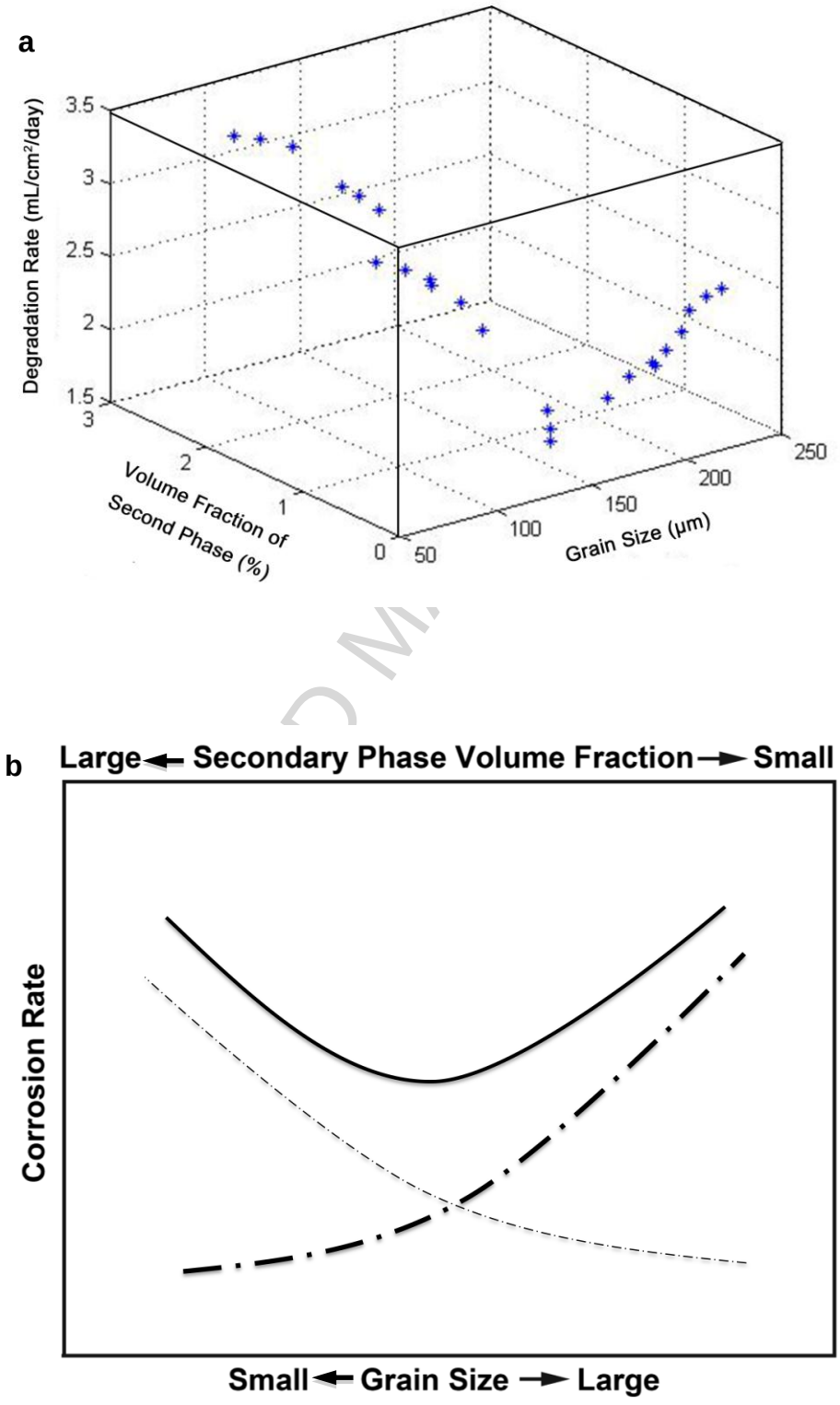

Figure 10 (a) The effects of temperature and time on the degradation rate in SBF against secondary phase volume fraction and grain size after different heat treatments; (b) Schematic drawing showing how the corrosion rate decreases with decreasing secondary phase content (thin chain-dashed curve) and increases with grain size (thick

chain-dashed curve) and the overall effect on the corrosion rate (indicated by solid curve).

4. Conclusions

As-cast Mg-3Zn-0.3Ca consists of Mg and (Mg + $Ca_2Mg_6Zn_3$) eutectic phase (globular and strip shaped). The degradation rate of the alloy changes after different heat treatments. The volume fraction of secondary phases and grain size are both key factors controlling the bio-corrosion rate of the alloy. The sample with the smallest grain size but the largest secondary phase volume fraction has the largest corrosion rate, because the secondary phase causes the galvanic corrosion which overshadows the beneficial effect of fine grain size. The sample with the lowest secondary phase volume fraction but the largest grain size also has a high corrosion rate is because the large grain size dominates (corrosion rate increases as grain size). The minimum corrosion rate was observed in the alloy heat-treated at 420 ^{o}C for 24 h which has a balanced secondary phase volume fraction and grain size.

Acknowledgement

Y. Lu is grateful for financial support from the University of Birmingham and a Ph.D scholarship from the China Scholarship Council.

References

[1] T. Okuma, *Magnesium and bone strength.* Nutrition, 2001. **17**(7-8): p. 679-680.

[2] F. Witte, V. Kaese, H. Haferkamp, E. Switzer, A. Meyer-Lindenberg, C.J. Wirth, and H. Windhagen, *In vivo corrosion of four magnesium alloys and the associated bone response.* Biomaterials, 2005. **26**(17): p. 3557-3563.

[3] R. Erbel, C. Di Mario, J. Bartunek, J. Bonnier, B. de Bruyne, F.R. Eberli, P. Erne, M. Haude, B. Heublein, M. Horrigan, C. Ilsley, D. Bose, J. Koolen, T.F. Luscher, N. Weissman, and R. Waksman, *Temporary scaffolding of coronary arteries with bioabsorbable magnesium stents: A prospective, non-randomised multicentre trial.* Lancet, 2007. **369**(9576): p. 1869-1875.

[4] E. Willbold, A.A. Kaya, R.A. Kaya, F. Beckmann, and F. Witte, *Corrosion of magnesium alloy AZ31 screws is dependent on the implantation site.* Materials Science and Engineering B - Advanced Functional Solid-State Materials, 2011. **176**(20): p. 1835-1840.

[5] H. Waizy, J.M. Seitz, J. Reifenrath, A. Weizbauer, F.W. Bach, A. Meyer-Lindenberg, B.

Denkena, and H. Windhagen, *Biodegradable magnesium implants for orthopedic applications.* Journal of Materials Science, 2013. **48**(1): p. 39-50.

[6] R.W. Revie and H.H. Uhlig, *Corrosion and corrosion control (Fourth edition),* 2008, Hoboken, New Jersey: John Wiley & Sons. p. 399.

[7] W.S. Loose, *Corrosion and Protection of Magnesium*, ed. L.M. Pidgeon, J.C. Mathes, and N.E. Woldmen1946: ASM International, Materials Park. p.173-260.

[8] M.M. Avedesian and H. Baker, *ASM Specialty Handbook: Magnesium and magnesium alloys,* 1999: ASM international. p.17.

[9] J.Z. Ilich and J.E. Kerstetter, *Nutrition in bone health revisited: A story beyond calcium.* Journal of the American College of Nutrition, 2000. **19**(6): p. 715-737.

[10] Y. Lu, A.R. Bradshaw, Y.L. Chiu, and I.P. Jones, *The role of β1' precipitates in the bio-corrosion performance of Mg–3Zn in simulated body fluid.* Journal of Alloys and Compounds, 2014. **614**: p. 345-352.

[11] K.D. Ralston, D. Fabijanic, and N. Birbilis, *Effect of grain size on corrosion of high purity aluminium.* Electrochimica Acta, 2011. **56**(4): p. 1729-1736.

[12] K.T. Liu and J.G. Duh, *Grain size effects on the corrosion behavior of Ni50.5Ti49.5 and Ni45.6Ti49.3Al5.1 films.* Journal of Electroanalytical Chemistry, 2008. **618**(1-2): p. 45-52.

[13] M. Hoseini, A. Shahryari, S. Omanovic, and J.A. Szpunar, *Comparative effect of grain size and texture on the corrosion behaviour of commercially pure titanium processed by equal channel angular pressing.* Corrosion Science, 2009. **51**(12): p. 3064-3067.

[14] K.D. Ralston, N. Birbilis, and C.H.J. Davies, *Revealing the relationship between grain size and corrosion rate of metals.* Scripta Materialia, 2010. **63**(12): p. 1201-1204.

[15] W. Zhou, T. Shen, and N.N. Aung, *Effect of heat treatment on corrosion behaviour of magnesium alloy AZ91D in simulated body fluid.* Corrosion Science, 2010. **52**(3): p. 1035-1041.

[16] L.M. Peng, J.W. Chang, X.W. Guo, A. Atrens, W.J. Ding, and Y.H. Peng, *Influence of heat treatment and microstructure on the corrosion of magnesium alloy Mg-10Gd-3Y-0.4Zr.* Journal of Applied Electrochemistry, 2009. **39**(6): p. 913-920.

[17] H.R. Bakhsheshi-Rad, M.R. Abdul-Kadir, M.H. Idris, and S. Farahany, *Relationship between the corrosion behavior and the thermal characteristics and microstructure of Mg-0.5Ca-xZn alloys.* Corrosion Science, 2012. **64**: p. 184-197.

[18] G.L. Song and A. Atrens, *Corrosion mechanisms of magnesium alloys.* Advanced Engineering Materials, 1999. **1**(1): p. 11-33.

[19] M.C. Zhao, M. Liu, G.L. Song, and A. Atrens, *Influence of the beta-phase morphology on the corrosion of the Mg alloy AZ91.* Corrosion Science, 2008. **50**(7): p. 1939-1953.

[20] T. Kokubo and H. Takadama, *How useful is SBF in predicting in vivo bone bioactivity?* Biomaterials, 2006. **27**(15): p. 2907-2915.

[21] G.L. Song, A. Atrens, and D.H. St. John, *Magnesium technology*, ed. J. Hryn2001, New Orleans, LA: TMS. p. 255.

[22] W.F. Ng, K.Y. Chiu, and F.T. Cheng, *Effect of pH on the in vitro corrosion rate of magnesium degradable implant material.* Materials Science and Engineering C - Materials for Biological Applications, 2010. **30**(6): p. 898-903.

[23] P.M. Jardim, G. Solorzano, and J.B. Vander Sande, *Precipitate crystal structure determination in melt spun Mg-1.5wt%Ca-6wt%Zn alloy.* Microscopy and Microanalysis,

2002. **8**(6): p. 487-496.

[24] D. Orlov, K.D. Ralston, N. Birbilis, and Y. Estrin, *Enhanced corrosion resistance of Mg alloy ZK60 after processing by integrated extrusion and equal channel angular pressing.* Acta Materialia, 2011. **59**(15): p. 6176-6186.

[25] N. Birbilis, K.D. Ralston, S. Virtanen, H.L. Fraser, and C.H.J. Davies, *Grain character influences on corrosion of ECAPed pure magnesium.* Corrosion Engineering Science and Technology, 2010. **45**(3): p. 224-230.

[26] G.R. Argade, S.K. Panigrahi, and R.S. Mishra, *Effects of grain size on the corrosion resistance of wrought magnesium alloys containing neodymium.* Corrosion Science, 2012. **58**: p. 145-151.

Highlights:

- Effects on the bio-corrosion behaviour are illustrated.
- Both of second phase volume fraction and grain size are key factors.
- A balanced secondary phase volume fraction and grain size is desirable.